

Uformer: A UNet-Transformer fused robust end-to-end deep learning framework for real-time denoising of lung sounds

Samiul Based Shuvo^a, Syed Samiul Alam^b and Taufiq Hasan^{a,c,*}

^a*m-Health Lab, Department of Biomedical Engineering, Bangladesh University of Engineering and Technology, Dhaka-1205, Bangladesh,*

^b*Department of Electrical and Electronic Engineering, Khulna University of Engineering & Technology (KUET), Khulna-9203, Bangladesh,*

^c*Center for Bioengineering Innovation and Design, Department of Biomedical Engineering, Johns Hopkins University, Baltimore, MD,*

ARTICLE INFO

Keywords:

Lung sound signal
Lung sound denoising
Signal denoising
Ambient sound interference
Deep neural networks
Denoising transformer

ABSTRACT

Objective: Lung auscultation is a valuable tool in diagnosing and monitoring various respiratory diseases. However, lung sounds (LS) are significantly affected by numerous sources of contamination, especially when recorded in real-world clinical settings. Conventional denoising models prove impractical for LS denoising, primarily owing to spectral overlap complexities arising from diverse noise sources. To address this issue, we propose a specialized deep-learning model (Uformer) for lung sound denoising. **Methods:** The proposed Uformer model is constituted of three modules: a Convolutional Neural Network (CNN) encoder module, dedicated to extracting latent features; a Transformer encoder module, employed to further enhance the encoding of unique LS features and effectively capture intricate long-range dependencies; and a CNN decoder module, employed to generate the denoised signals. An ablation study was performed in order to find the most optimal architecture. **Results:** The performance of the proposed Uformer model was evaluated on lung sounds induced with different types of synthetic and real-world noises. Lung sound signals of -12 dB to 15 dB signal-to-noise ratio (SNR) were considered in testing experiments. The proposed model showed an average SNR improvement of 16.51 dB when evaluated with -12 dB LS signals. Our end-to-end model, with an average SNR improvement of 19.31 dB, outperforms the existing model when evaluated with ambient noise and fewer parameters. **Conclusion:** Based on the qualitative and quantitative findings in this study, it can be stated that Uformer is robust and generalized to be used in assisting the monitoring of respiratory conditions.


1. Introduction


The respiratory system plays a pivotal role in human health, making it crucial to diagnose respiratory diseases accurately and monitor patient conditions. Pulmonary disorders are the third leading cause of death in the world(1). In this context, lung sounds serve as a valuable tool for physicians. They offer insights into both the normal physiological processes and potential pathologies within the respiratory system(2). Generally, these sounds can be classified into normal and abnormal categories (3). Auscultation, the practice of listening to physiological sounds such as those of the lungs, is a technique often used by physicians and clinicians to detect respiratory illnesses such as Asthma, Chronic Obstructive Pulmonary Disease (COPD), Bronchiolitis, and Bronchitis. Despite its significance, this method often encounters challenges due to inter-listener variability, where different individuals might interpret the sounds differently. There has been an emerging research trend toward computer-based lung sound (LS) analysis to address this subjective inconsistency. For instance, by utilizing electronic stethoscopes, this technological advancement provides a more objective and consistent method to evaluate lung functions (4; 5).

However, LS recordings, particularly in real-world environments, are invariably subject to various interferences. These include heart sounds, microphone contact noise, muscle contractions, noises from other medical equipment, conversations, mobile phones, and assorted ambient disturbances. Such interference can undermine the precision of computer-based LS analyses, creating a risk of misdiagnoses or missed diagnoses. As a result, noise reduction or denoising becomes a critical component in LS signal processing in electronic stethoscopes. Nevertheless, this task is challenging. The noise is unpredictable and dynamic and can differ based on an individual's physical condition. A primary obstacle lies in the temporal and spectral overlap between the essential LS signals and the intrusive noise sources (6; 7; 8).

LS signal denoising methodologies can be primarily divided into classical model-based and learning-based denoising methods. One prevalent technique within the classical model-based category for LS denoising is wavelet-based thresholding methods. These have exhibited commendable performance, especially when the noise-free signal is missing (9; 10). (10) integrated FIR band-pass, modified wavelet, and adaptive filters to segregate ambient noise and heart sounds from LS signals. Meanwhile, an alternate approach documented in (11) employed the Daubechies wavelet, specifically with four coefficients, to eliminate noise. A notable drawback of traditional wavelet-based methods is the introduction of artifacts, such as Gibbs oscillations and noise spikes, particularly around signal discontinuities (12).

*Corresponding author

 sbshuvo@bme.buet.ac.bd (S.B. Shuvo); syed.samiul.alam@ieee.org (S.S.A.)

 taufiq.hasan@jhu.edu; taufiq@bme.buet.ac.bd (Taufiq Hasan)
ORCID(S): 0000-0002-5035-2114 (S.B. Shuvo); 0000-0002-3742-6692 (S.S.A.); 0000-0002-6142-3344 (Taufiq Hasan)

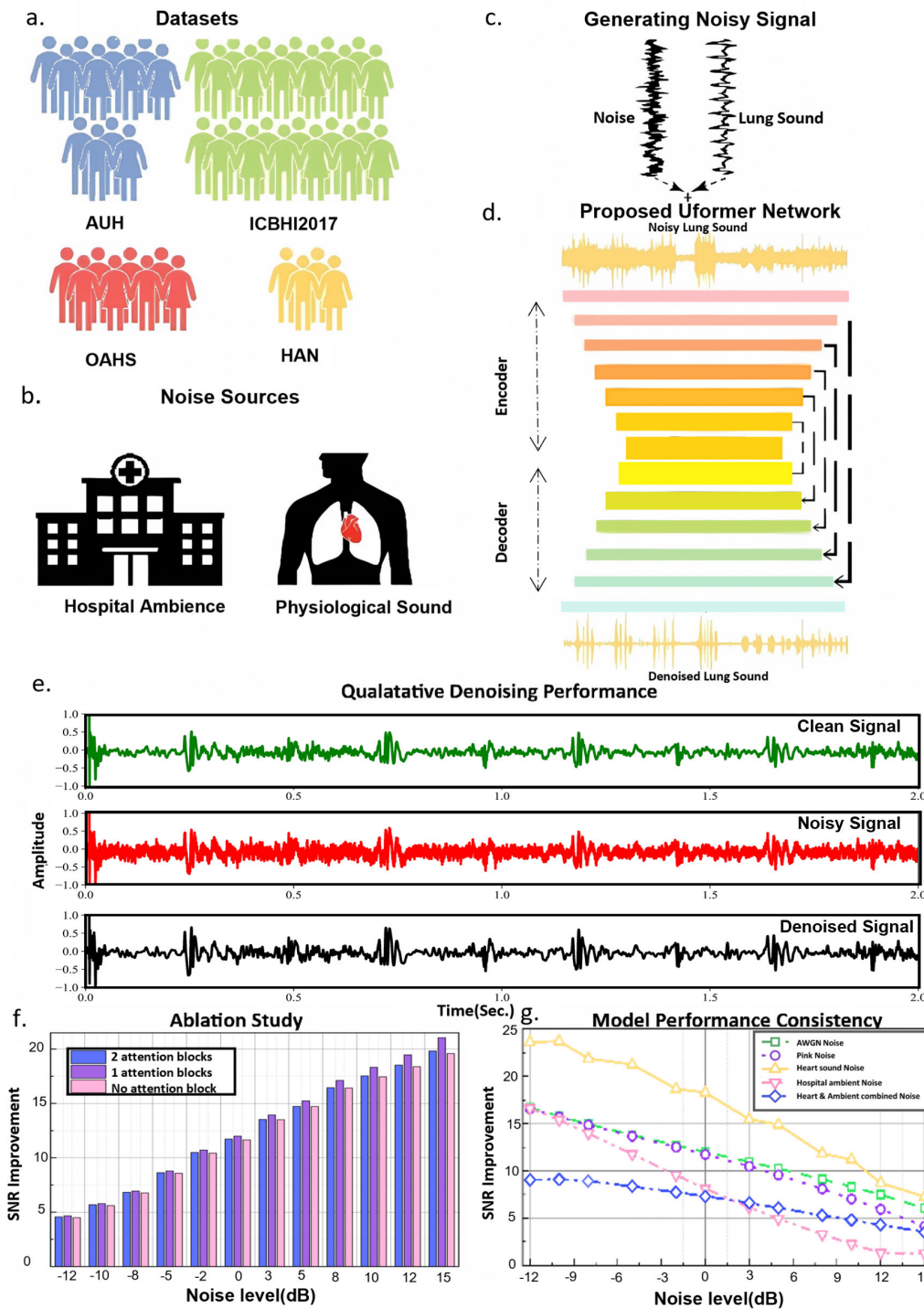


Figure 1: (a) The schematic represents datasets of different signals (LS, HS, and hospital noise) utilized in this research (b) The real world noise sources (c) Generation of input noisy signals (d) Schematic of the proposed Uformer model (e) A qualitative analysis of proposed model: Noisy signal, clean signal, and denoised signal (f) Ablation study: Comparisons of SNR improvement of different variations of the proposed architecture (Uformer+, Uformer, and Noformer) for LS corrupted with WGN noise (g) Performance of the proposed Uformer model for different types of noise in terms of SNR improvement.

Empirical Wiener filtering was integrated within the wavelet transform domain to alleviate these constraints. However, this technique needs the use of dual wavelet transform bases, and the specific combinations of wavelet bases influence its

denoising effectiveness used (13; 14; 15; 16). In a separate study (17), Empirical Mode Decomposition (EMD) was employed to dissect the LS signal into its constituent components. The objective was to suppress the intrusion of heart

Algorithm 1: Lung sound preparation

```

Input :  $\mathbb{L}_c$ 
Output:  $\mathbb{L}_{c,8k,1s}$ 
1 for  $S_i \leftarrow 1$  to  $\text{length}(\mathbb{L}_c)$  do
2    $S_{i8k} \leftarrow \text{Resample at } s_r$ 
3    $iter_{int} \leftarrow \text{Int}(S_{i8k}/s_r)$  // Number of complete
      1 second segment(s) from a single lung sound
4   if  $iter_{int} \neq 0$  then
5      $seg_{start} \leftarrow 0, seg_{end} \leftarrow seg_{start} + s_r$ 
6     for  $i \leftarrow 1$  to  $iter_{int}$  do
7        $S_{i8k,1s} \leftarrow S_{i8k}[seg_{start} : seg_{end}]$ 
8       append  $S_{i8k,1s}$  in  $\mathbb{L}_{c,8k,1s}$ 
9        $seg_{start} \leftarrow seg_{end}$ 
10    end
11  else
12     $inc \leftarrow (\frac{S_{i8k}}{s_r} - iter_{int})$  // Number of
      complete 1 second segment(s) from a
      single lung sound
13    if  $inc \geq 0.5$  and  $iter_{int} == 0$  then
14       $res \leftarrow S_{i8k} | S_{i8k}$  // Stack signals to
      increase the length
15    end
16    if  $inc \geq 0.5$  and  $iter_{int} \neq 0$  then
17       $res \leftarrow S_{i8k}[seg_{start} :$ 
       $end] | S_{i8k}[seg_{start} : end]$  // Stack
      signals to increase the length
18    end
19    append  $res[start : s_r]$  in  $\mathbb{L}_{c,8k,1s}$ 
20  end
21 end

```

sounds into lung sounds, and the results were promising across both frequency and time-frequency domains. Another method (18) harnessed local projection to diminish acoustic noise commonly found in hospital surroundings. The research study in (19) combined EMD with Hurst Analysis and spectral subtraction to filter out high-frequency noise disturbances from LS signals across various settings. (20) opted for the Savitzky-Golay filter to neutralize varying intensities of Gaussian noise evident in the LS signal. Recent innovations have steered towards adaptive techniques for the dynamic elimination of noise from lung sounds. In (21), the authors introduced an automated multiband method to eliminate clinical noise from the LS signal. Interferences from heart sounds, which often have spectral overlap with lung sounds, were tackled in (22) with the formulation of a Normalized Least-Mean-Square (NLMS) method. This ensured an adaptive distinction between the two sound types.

Transitioning to the realm of artificial intelligence, the integration of deep learning is becoming increasingly prevalent in denoising various physiological signals, including electroencephalogram (EEG) (23; 24), electrocardiogram (ECG) (25; 26), and phonocardiogram (PCG) (27; 28) . In this context, research works (6) and (7) incorporated

Algorithm 2: Generation of Noisy Lung Sound With WGN

```

Input :  $\mathbb{L}_{c,8k,1s}$  - Clean 8kHz lung sound signal of
      1s
1  $\mu_{noise} \leftarrow 0$ 
2 for  $S_i \leftarrow 1$  to  $\text{Length}(\mathbb{L}_{c,8k,1s})$  do
3    $SNR_{Desired} \leftarrow$ 
       $[-12, -10, -8, -5, -2, 0, 3, 5, 8, 10, 12, 15]$ 
4   for  $j \leftarrow 1$  to  $\text{length}(SNR_{Desired})$  do
5      $SNR_{Desired_j} \leftarrow SNR_{Desired}[j]$ 
6      $\mathbb{P}_{S_i} \leftarrow \frac{S_i^2}{\text{length}}$ 
7      $\mathbb{P}_N \leftarrow \mathbb{P}_{S_i}^2 * 10^{\frac{-SNR_{Desired_j}}{10}}$ 
8      $\mathbb{N}_j \leftarrow \eta(\mu_{noise}, \mathbb{P}_{Noise})$ 
9      $S_{Noisy_i} \leftarrow S_i + \mathbb{N}_j$ 
10    Write  $S_{Noisy_i}$  in a .wav file
11  end
12 end

```

Algorithm 3: Generation of Noisy Lung Sound With pink noise

```

Input :  $\mathbb{L}_{c,8k,1s}$  - Clean 8kHz lung sound signal of
      1s
1  $\mu_{noise} \leftarrow 0$ 
2 for  $S_i \leftarrow 1$  to  $\text{Length}(\mathbb{L}_{c,8k,1s})$  do
3    $SNR_{Desired} \leftarrow$ 
       $[-12, -10, -8, -5, -2, 0, 3, 5, 8, 10, 12, 15]$ 
4   for  $j \leftarrow 1$  to  $\text{length}(SNR_{Desired})$  do
5      $SNR_{Desired_j} \leftarrow SNR_{Desired}[j]$ 
6      $\mathbb{N} = \xi(\sqrt{\frac{1}{s_r}})$  //generating pink noise with
      unit amplitude
7      $\mathbb{P}_{S_i} \leftarrow \frac{S_i^2}{\text{length}}$ 
8      $\mathbb{P}_{Noise} \leftarrow \frac{Power_{\mathbb{N}_j}^2}{\text{length}} * 10^{\frac{-SNR_{Desired_j}}{10}}$ 
9      $\mathbb{N}_j \leftarrow \eta(\mu_{noise}, \mathbb{P}_{Noise})$ 
10     $S_{Noisy_i} \leftarrow S_i + \mathbb{N}_j$ 
11    Write  $S_{Noisy_i}$  in a .wav file
12  end
13 end

```

deep learning frameworks to denoise LS signals. The study (6) merged wavelet transform with an artificial neural network (DWT-ANN) for this purpose. Their outcomes reflected that the DWT-ANN outperformed the standalone wavelet transform method. Their methodology utilized synthetic Gaussian white noise at varying signal-to-noise ratios (SNRs) to validate their algorithm. The artificial nature of this noise does not mimic the intricate and unpredictable nature of noise in real-world clinical settings. Similarly, (7) unveiled a method featuring a two-stage process that integrates adaptive noise cancellation (ANC) with deep neural networks (DNNs) to filter out ambient noises and retain the

Table 1
Specifications of training and testing datasets with different noise levels

Split	Dataset Name	Name	Noise Type	Noise level(dB)	No. of samples (1s segment)
Training(90%) Validation(10%)	ICBHI-2017 (731 recordings)	ICBHI-1 ICBHI-2 ICBHI-3 ICBHI-4	WGN Pink Noise Heart Sound Noise Ambient Noise	[-10,-5,0,5,10,15]	92556
Testing	ICBHI-2017 (186 recordings)	ICBHI_inf-1 ICBHI_inf-2 ICBHI_inf-3 ICBHI_inf-4	WGN Pink Noise Heart Sound Noise Ambient Noise	[-10,-5,0,5,10,15], [-12,-8,-2,3,8,12] (unseen noise level)	25410
	AUH Lung Sound Dataset (55 recordings)	AUH-1 (unseen dataset)	WGN		9745

Algorithm 4: Get noise function

```

1 Function GetNoise(type):
2   if type == heart then
3      $\mathbb{N} \leftarrow \text{Randomly select a heart sound}$ 
4      $\mathbb{N}_{8k} \leftarrow \text{Resample } \mathbb{N} \text{ at } 8k\text{Hz}$ 
5     return  $\mathbb{N}_{8k}$ 
6   end
7   if type == ambient then
8      $\mathbb{N}_{heart} \leftarrow \text{Randomly select a heart sound}$ 
9      $\mathbb{N}_{heart_{8k}} \leftarrow \text{Resample } \mathbb{N}_{heart} \text{ at } 8k\text{Hz}$ 
10     $\mathbb{N}_{hospital} \leftarrow$ 
11     $\text{Randomly select a hospital sound}$ 
12     $\mathbb{N}_{hospital_{8k}} \leftarrow \text{Resample } \mathbb{N}_{hospital} \text{ at } 8k\text{Hz}$ 
13    return  $0.7 * \mathbb{N}_{heart_{8k}} + 0.3 * \mathbb{N}_{hospital_{8k}}$ 
14  end
    
```

functional signal components. Their approach attempted to simulate real-world scenarios more closely by introducing environmental and hospital noises to clean lung sounds. Nevertheless, the issue of heart sounds interfering with lung sounds due to their anatomical proximity is a challenging real-world problem that was not fully addressed. A pivotal limitation of both methodologies is the absence of an end-to-end approach. By combining signal processing with deep learning methodologies, they inadvertently introduced latency in real-time signal processing.

Given the limitations and challenges present in existing works, we introduce an end-to-end self-attention-enabled "Uformer" architecture designed to proficiently denoise lung sounds. This holistic approach leverages long-range contextual information from the encoder and integrates it with spatial specifics during the decoding process, resulting in the generation of precise denoised outputs by the decoder. The performance of the proposed model is rigorously assessed using a diverse set of challenging real-world noise types, with a particular emphasis on relevant noise like heart sounds. A complete flow diagram of our study is shown in Fig. 1.

The major contributions of our work are as follows:

Algorithm 5: Generation of Noisy Lung Sound With heart sound and ambient noise

```

Input :  $\mathbb{L}_{c,8k,1s}$  - Clean 8kHz lung sound signal of 1s
1  $\mu_{noise} \leftarrow 0$ 
2 for  $S_i \leftarrow 1$  to  $\text{Length}(\mathbb{L}_{c,8k,1s})$  do
3    $SNR_{Desired} \leftarrow$ 
4    $[-12, -10, -8, -5, -2, 0, 3, 5, 8, 10, 12, 15]$ 
5   for  $j \leftarrow 1$  to  $\text{length}(SNR_{Desired})$  do
6      $SNR_{Desired_j} \leftarrow SNR_{Desired}[j]$ 
7      $noiseType = [ehearte, eambiente]$ 
8     for  $t \leftarrow 1$  to  $\text{length}(noiseType)$  do
9        $\mathbb{N} \leftarrow \text{GetNoise}(noiseType[t])$ 
10       $\mathbb{P}_{S_i} \leftarrow \frac{S_i^2}{\text{length}}$ 
11       $\mathbb{P}_{Noise} \leftarrow \frac{\text{Power}_{\mathbb{N}_i}^2}{\text{length}}$ 
12       $SF \leftarrow \frac{\mathbb{P}_{Signal}}{\mathbb{P}_{Noise}} * 10^{\frac{-SNR_{Desired_j}}{10}}$ 
13       $\mathbb{N}_{scaled} \leftarrow \sqrt{SF} * \mathbb{N}$ 
14       $S_{Noisy_i} \leftarrow S_i + \mathbb{N}_{scaled}$ 
15      Write  $S_{Noisy_i}$  in a .wav file
16    end
17  end
    
```

- We introduced a novel "Uformer" model tailored specifically for the efficient denoising of lung sounds. This architecture seamlessly combines convolutional and transformer structures in a dual-encoder-decoder framework.
- We integrated a multi-head attention mechanism into the encoder to enhance the model's ability to handle non-deterministic and overlapping noise in lung sounds. This mechanism captures long-range dependencies, proving essential for addressing complex noise scenarios.

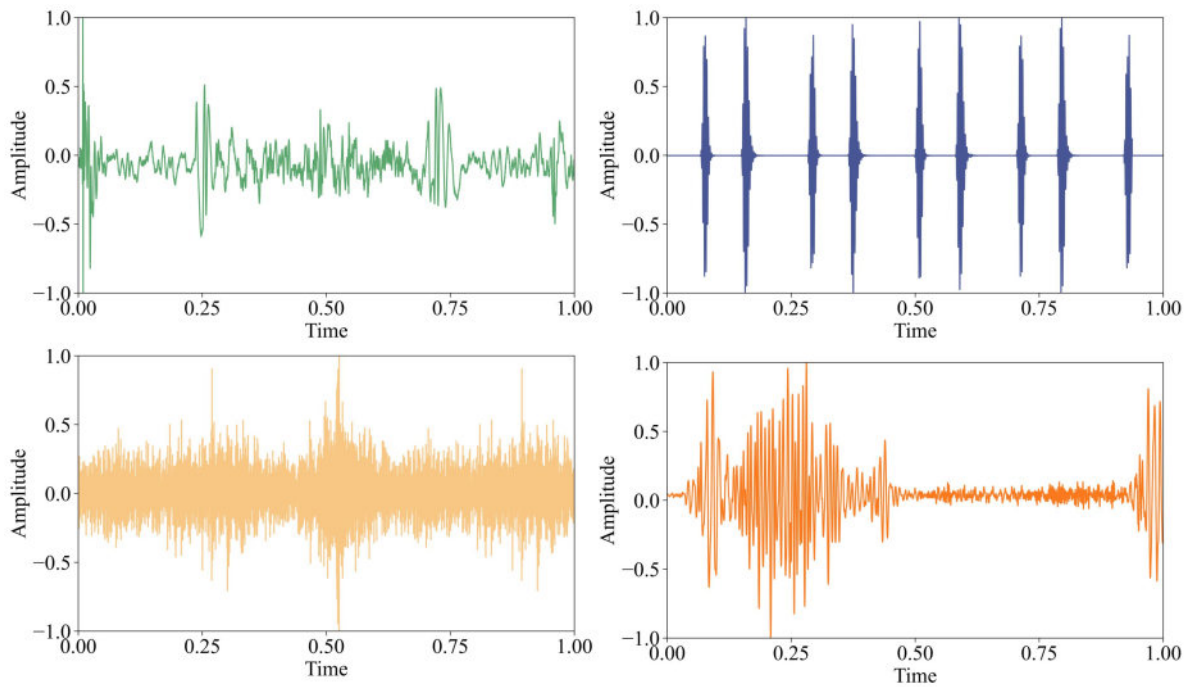


Figure 2: Representative signal of (a) Lung sound, (b) Heart sound signal of OAHS, (c) Hospital ambient sound signal of HAN and (d) Hospital & Heart sound combined noise signal

- Conducted experimental validation by infusing lung sounds with diverse noisy conditions, including WGN, pink noise, heart sound noise, and real-world heart and hospital sounds to simulate challenging and varied scenarios. The denoiser’s performance was extensively evaluated across a spectrum of signal-to-noise ratios (SNRs) during both the training and testing phases. Moreover, the experimentation spanned a wide range of datasets for training and testing, affirming the generalizability and robustness of the proposed Uformer architecture.

The structure of this paper is as follows: In Section 2, we present a comprehensive exploration of data resources and an overview of the noisy signal generation scheme. Section 3 provides an in-depth explanation of our proposed method and details of the experimental setup and the evaluation metrics employed. Section 5 describes the experimental details, presenting both qualitative and quantitative analyses of the obtained results. Finally, in Section 6, we summarize our findings and conclude with remarks emphasizing future directions.

2. Materials and Methods

2.1. Dataset Description

In this study, two different LS datasets were used. The International Conference on Biomedical Health Informatics (ICBHI) 2017 dataset (29) was considered as the primary LS dataset. The secondary independent test LS dataset was the Abdullah University Hospital (AUH) dataset (30). The heart sounds and hospital ambient sounds were utilized as noise

and collected from the Open Access Heart Sound (OAHS) and Hospital Ambient Noise (HAN) datasets. A brief description of the datasets is discussed in this subsection.

2.1.1. ICBHI 2017 Dataset

The International Conference on Biomedical Health Informatics (ICBHI), published a benchmark dataset of lung auscultation sounds for public use in 2017. This dataset was collected by two research groups from Greece and Portugal, containing a total recording of 5.5 hours, sampled at 4KHz, 14KHz, and 44.1KHz with annotated respiratory cycles from 126 patients with 920 recordings (29). The data length of each signal varies from 10sec to 90sec. The dataset includes seven classes, namely, Upper Respiratory Tract Infection, Lower Respiratory Tract Infection, Chronic Obstructive Pulmonary Disease, Bronchiolitis, Bronchiectasis, Pneumonia, and Asthma. A detailed dataset description can be found in (31). In this work, we have utilized 80% of the data for training and 20% of the data for testing our models, and among the training set, 10% of the data were set aside for validation.

2.1.2. AUH Lung Sound Dataset

The AUH dataset contains respiratory signals from 112 Middle Eastern subjects (77 unhealthy and 35 healthy) aged 21-90, collected from King Abdullah University Hospital, Ramtha, Jordan. Each recording is 5-30 seconds long. The dataset has respiratory signals of eight different lung conditions: asthma, pneumonia, BRON, COPD, heart failure, lung fibrosis, pleural effusion, and normal. A single-channel stethoscope was used to record the LS signals. All signals

were collected at a sampling rate of 4 KHz using a 16-bit quantizer. The detailed description of the dataset can be found in (30).

2.1.3. Open Access Heart Sound Dataset

In the present work, the OAHS dataset encompassed five distinct categories: Mitral Regurgitation (MR), Aortic Stenosis (AS), Mitral Stenosis (MS), Mitral Valve Prolapse (MVP), and Normal (N). The signals were collected from diverse sources, including websites, CDs, and books (32). The dataset comprises a total of 1,000 audio recordings, with each entry containing three complete cardiac cycles of clear heart sounds sampled at 8kHz as single-channel signals. Furthermore, each category is represented by 200 individual recordings. The processes of sampling, editing, and file conversion were facilitated using the Cool Edit software. Further details about the OAHS dataset can be found in (32).

2.1.4. HAN Dataset

This dataset has been prepared using a non-copyrighted video from YouTube of 68 minutes of a busy hospital where the audio occurrences were recorded from different places such as the waiting room, corridor, etc. The dataset contains 562 samples, each of which has a duration of 5 seconds. Further details of the dataset can be found in (27).

2.2. Data Preprocessing

2.2.1. Lung Sound Preparation

The frequency spectrum of the LS signals usually resides between 50 Hz to 2500 Hz (2). The LS signals utilized in this work were filtered with a 6th-order Butterworth filter to mimic a ground truth clean signal. Then, LS signals were resampled at 8KHz to ensure consistency and normalized within the range of $[-1, 1]$ (33). In order to reduce complexity, each signal was converted into multiple segments using a non-overlapping window of 1 second. The steps involving LS preparation are discussed in Algo. 1 where \mathbb{L}_c and $\mathbb{L}_{c,8k,1s}$ are unsegmented LS signals resampled segmented LS signals, respectively. S_i and $S_{i,8k}$ are single LS signals and single resampled segmented LS signals, respectively.

2.2.2. Generating Synthetic Noisy Signals

We initially divided the ICBHI2017 dataset into training and testing sets with a ratio of 75% for training and 25% for testing. Then, to assess the denoiser model's robustness for lung sounds, we introduced various types of noise to the original signals, simulating real-world scenarios and challenges. The noise types used for this evaluation included:

White Noise and Pink Noise: In contrast to the controlled and reduced noise levels typically encountered in acoustic labs, the real-world environment of operating rooms introduces significant challenges. High noise levels originate from surgical devices, ventilation machines, conversations, alarms, and other sources, which make analyzing lung sounds more complex. Additional noise can be introduced by the sliding motions of stethoscope diaphragms, resulting

from physician adjustments or patient agitation, further complicating the diagnostic process.

In this context, noise elimination techniques become essential to mitigate the detrimental impact of such noise. Environmental noises are often considered colored noises. Therefore, we approximated background noise as additive white Gaussian noise (WGN) and Pink Noise when capturing lung sounds. WGN and pink noise can also be approximated for various real-world noises, including fan, air conditioner noise, and other static sounds from various medical devices (34). WGN, in particular, is commonly used in deep learning-based classification and denoising tasks due to its uniform distribution of noise power across all frequencies (34; 35; 36; 37). While WGN is an ideal form of noise, Pink Noise closely resembles the characteristics of real-world noise. Consequently, in our evaluation, we considered both WGN and pink noise to assess the denoiser model's performance in the presence of synthetic and real-world noise.

We contaminated LS signals from the ICBHI 2017 Dataset to WGN and Pink Noise at various SNRs during the model's training to evaluate our enhancement algorithm comprehensively. These SNRs encompassed a wide range, including -10 dB, -5 dB, 0 dB, 5 dB, 10 dB, and 15 dB.

In addition to these SNRs, we sought to assess the model's adaptability to the unseen noise levels not used in the training phase. Therefore, we conducted an evaluation using LS signals at SNRs of -12 dB, -8 dB, -2 dB, 3 dB, 8 dB, and 12 dB, further expanding the scope of our assessment.

To further evaluate the model's robustness and its ability to adapt to noise introduced from external datasets, we conducted tests using the AUH Lung Sound Dataset. This evaluation involved the introduction of WGN at SNRs of -12 dB, -10 dB, -8 dB, -5 dB, -2 dB, 0 dB, 3 dB, 5 dB, 8 dB, 10 dB, 12 dB, and 15 dB. This comprehensive evaluation approach ensured that our denoiser model could effectively handle a wide array of noise levels, both from its training and external independent test datasets, making it a versatile and reliable solution for addressing noisy medical environments. The step-by-step process of inducing WGN and pink noise in LS is illustrated in Algo. 2 and 3.

Heart Sound Noise and Hospital Ambient Noise:

Though denoiser models are typically trained and evaluated on synthetic noises, real-world noises are often more complex, including spatially-correlated, spatially-variant, device-dependent, and signal-dependent components (38). Therefore, evaluating models solely based on synthetic noise may not suffice. In the case of lung sounds, the primary source of signal deterioration is the presence of heart sounds.

Heart sounds, specifically the first (S1) and the second (S2) components of normal heart sound recordings, fall within the frequency range of 20 Hz to 150 Hz (39). This frequency range overlaps with typical lung sounds, which may vary between 30 Hz and 1000 Hz. Distinguishing pure respiratory signals from heart sounds can be challenging, as both signals originate from anatomical sites close to each other (40). In addition to heart sound noise, hospital

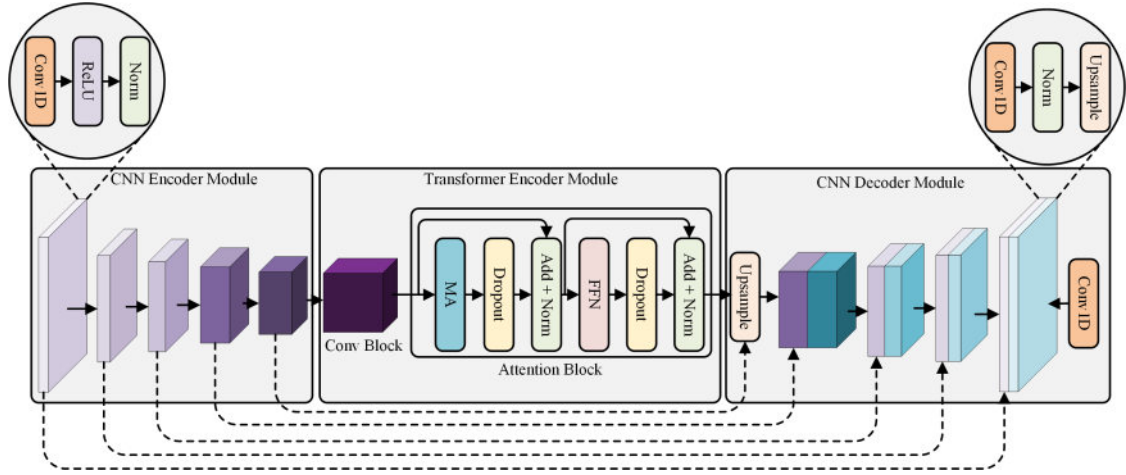


Figure 3: The proposed Uformer Network

ambient noise contributes to the degradation of respiratory signals. Sources of hospital ambient noise include human conversation, intestinal activity, stethoscope movement, and sensor variations (41).

To address the challenge posed by real-world noises, we trained and evaluated our denoiser model on both LS signals with heart sound noise and a combination of heart sound noise and hospital ambient noise. We used the Open-Access Heart Sound (OAHS) dataset for heart sound noise and the Hospital Ambient Noise (HAN) dataset for hospital ambient noise. During the training phase, we introduced these noise types at various signal-to-noise ratios (SNRs) into the LS signals from the ICBHI 2017 Dataset. The SNRs considered for training were -10 dB, -5 dB, 0 dB, 5 dB, 10 dB, and 15 dB. Additionally, our model's adaptability to unseen noise levels was thoroughly assessed by subjecting it to LS signals at SNRs of -12 dB, -8 dB, -2 dB, 3 dB, 8 dB, and 12 dB. Algo. 4 and 5 delineates the step-by-step process of inducing heart sound and ambient noise.

A brief overview of the specifications of the training and testing datasets demonstrated in Table 1.

3. Uformer Architecture

Our proposed Uformer model is designed to perform denoising on noisy LS. The architecture, tailored for temporal domain signals, integrates three principal components: a CNN encoder module for latent features extraction, a transformer encoder module to refine the encoding of distinctive lung sounds and capture fine long-range dependencies, and a CNN decoder to produce enhanced denoised signals (see detailed visual description in Fig. 3). Detailed insights into each module are given in the following subsections.

3.1. Input Formulation

The noisy LS signals are represented as a tensor $x \in \mathbb{R}^{N \times C}$ where $C = 1$ corresponds to the number of channels, and $N = 8000$ represents the count of noisy samples. The entire dataset can be articulated as $X = \{x_1, x_2, \dots, x_N\}$.

3.2. CNN Encoder Module

The CNN encoder module symbolized as E^{CNN} , draws inspiration from the U-Net design. It comprises five recurring blocks, E_b^{CNN} . Each block consists of a Conv1d-ReLU pair, utilizing a kernel size of 31 and a stride of 2. Following these operations, a Batch-normalization layer is applied. For a given input signal x , each CNN encoder block outputs $f_{a,n} = \{f_{a1,n1}, f_{a2,n2}, \dots, f_{a5,n5}\}$, where $f_{a,n} \in \mathbb{R}^{N_a \times C_a}$ denotes the feature map at each block level. Here, 'a' ranges from 1 to 5, and $n \in \{16, 32, 32, 64, 64\}$ signifies the filter count. N_a and C_a represent the feature map size and channel number at level a , respectively. The final feature map $f_{a5,n5} = z'$ serves as the input for the transformer encoder module.

3.3. Transformer Encoder Module

The transformer encoder module, denoted as E^{Trans} , is structured into two blocks: the convolutional block, E_c^{Trans} , and the attention block, E_{att}^{Trans} . To ensure minimal memory usage, E_c^{Trans} further compresses the output feature map z' from E^{CNN} . The E_c^{Trans} block incorporates Conv1d-ReLU operations with 128 filters, using a stride of 2, succeeded by Batch-normalization layers. The E_{att}^{Trans} block comprises two sub-layers: the first employs a multi-head self-attention mechanism (MA), and the second integrates a position-wise, fully connected feed-forward network.

Given the current representations $\mathbf{m}_t = \{\mathbf{m}_1, \mathbf{m}_2, \dots, \mathbf{m}_N\}$ from the convolutional block, the refined representation \mathbf{n}_t is determined as:

$$\begin{aligned} n_t &= \mathcal{MA}(m_1, m_2, \dots, m_N) \\ &= \left[\mathcal{A}_1(Q, K, V)(m_t) \oplus \mathcal{A}_2(Q, K, V)(m_t) \right. \\ &\quad \left. \mathcal{A}_i(Q, K, V)(m_t) \right] W_o \end{aligned} \quad (1)$$

The attention function \mathcal{A} is defined as:

$$\mathcal{A}(\mathbf{Q}, \mathbf{K}, \mathbf{V}) = \mathcal{SM} \left(\frac{\mathbf{W}_Q \mathbf{W}_K^T}{\sqrt{d_k}} \right) \mathbf{W}_V \quad (2)$$

Where \mathcal{SM} signifies softmax activation, and \mathbf{W}_Q , \mathbf{W}_K , and \mathbf{W}_V are weight matrices for queries, keys, and values respectively. Dimensions of queries, keys d_k and values is 25.

The sub-layer's output is then calculated as:

$$\mathbf{g} = \mathcal{LN}(\mathbf{m}_t + \mathcal{MA}(\mathbf{m}_t)) \quad (3)$$

Where \mathcal{LN} symbolizes the layer normalization layer.

The second sub-layer employs two dense layers (D) with ReLU activation in between, each containing 128 nodes. Residual connections link the two sub-layers, succeeded by layer normalization. The sub-layer's output is represented as:

$$\mathbf{h} = \mathcal{LN} \left(D(\text{ReLU}(D(\mathbf{g}))) + \mathbf{g} \right) \quad (4)$$

Subsequently, the feature map undergoes upsampling (factor of 2) and is concatenated with $\mathbf{f}_{a5,n5}$ to yield the final encoded feature map $\mathbf{z} = E^{\text{Trans}}(z')$.

3.4. CNN Decoder Module

The CNN decoder module, symbolized as D^{CNN} , contains 4 blocks, termed D_b^{CNN} blocks, where $b=1$ to 4. Each block integrates pairs of Conv1d-ReLU operations using a kernel size of 31 and a stride of 1. These operations are followed by batch normalization and Upsample layers with a scale factor of 2.

The encoder-derived feature map, \mathbf{z} , serves as the decoder input. It undergoes upsampling and passes through the decoder blocks to reconstruct high-resolution signals. Each feature map of a CNN decoder block is designated as

$$d_{a,n} = \{d_{a1,n1}, d_{a2,n2}, \dots, d_{a4,n4}\}.$$

where a denotes the block level (from 1 to 4), and n relates to the filter count in each convolutional layer, with $n \in \{64, 32, 32, 32\}$. Skip connections bridge the encoder and decoder to ensure the retention of intricate details, significantly enhancing denoised LS reconstruction. The combined feature maps, labeled as $k_{a,n}$, are expressed as:

$$k_{a,n} = h_{a,n} \oplus f_{5-a,n} \quad (5)$$

where \oplus represents concatenation of two vectors.

3.5. Output Formulation

The final feature map from the decoder module, $k_{4,32}$, traverses a concluding Conv1d-Tanh layer with a single filter. This process yields the ultimate denoised signal $\hat{y} = \{\hat{y}_1, \hat{y}_2, \dots, \hat{y}_N\}$ where $\hat{y} \in \mathbb{R}^{N \times 1}$ and $N = 8000$.

4. Experimental Setup

4.1. Loss Function

The Mean Squared Error (MSE), which we used in our training process, quantifies the dissimilarity between the denoised signal and the ground truth signal. This function measures the average squared difference between the corresponding samples of the denoised signal \hat{y} and the clean input signal y . Minimizing the MSE encourages our model to produce denoised signals that closely match the true, noise-free signal. The MSE loss can be expressed as follows :

$$\mathcal{L}_{\text{MSE}} = \frac{1}{N} \sum_{i=1}^N (x_i - y_i)^2 \quad (6)$$

where N represents the total number of samples in the signals, y_i is the i th sample of the clean lung sound signal, \hat{y}_i is the i th sample of the denoised LS signal.

4.2. Hyperparameters

For training both models, we employ the Adam (42), with an initial learning rate (lr) set to 10^{-4} and a batch size of 512. We opt for the Adam optimizer due to its superior efficacy compared to other optimization methods, and its stochastic momentum-based approach is chosen to expedite the model training process (43).

4.2.1. Hardware

Our models have been developed using Keras and TensorFlow 2.0 and trained using an Intel 12th Gen Core i7-12700F 5GHz CPU, 128 GB RAM, and a GeForce RTX 4090 GPU with 24 GB VRAM.

4.3. Evaluation Metrics

4.3.1. Signal-to-Noise Ratio (SNR)

Signal-to-Noise Ratio (SNR) is a primary metric for evaluating noise reduction performance in LS denoising. It is defined as follows:

$$\begin{aligned} \mathcal{E}_{\text{SNR (dB)}} &= 10 \log_{10} \left(\frac{P_{\hat{y}}}{P_n} \right) \\ &= 10 \log_{10} \left(\frac{\sum_{t=1}^N \hat{y}[t]^2}{\sum_{t=1}^N (y[t] - \hat{y}[t])^2} \right) \end{aligned} \quad (7)$$

where $P_{\hat{y}}$ and P_n represent the power of the denoised LS signal and noise, respectively. Also, $\hat{y}[t]$ and $y[t]$ indicate the t^{th} sample of the denoised LS signal and the clean LS signal, respectively, while N denotes the total number of samples in the signal and noise.

4.3.2. Root-Mean-Squared Error (RMSE)

Root-mean-squared error (RMSE) is commonly used to measure the difference between the intended and actual signals. A lower RMSE indicates a smaller difference. The RMSE between the clean and denoised LS recordings is calculated as:

$$\mathcal{E}_{\text{RMSE}} = \sqrt{\frac{1}{N} \sum_{t=1}^N (y[t] - \hat{y}[t])^2} \quad (8)$$

Table 2

Ablation study results comparing the performance of different attention mechanisms

Noise Level (in dB)	Model Configurations								
	Uformer+			Uformer			Noformer		
	PRED_SNR	PRD	RMSE	PRED_SNR	PRD	RMSE	PRED_SNR	PRD	RMSE
-12	4.5772	0.9750	0.0583	4.6709	0.9710	0.0579	4.5002	0.9770	0.0586
-10	5.6953	0.9583	0.0512	5.7871	0.9543	0.0509	5.6226	0.9603	0.0515
-8	6.8450	0.9338	0.0447	6.9504	0.9298	0.0445	6.7811	0.9358	0.0450
-5	8.6335	0.8759	0.0361	8.7927	0.8719	0.0359	8.5871	0.8779	0.0363
-2	10.4977	0.7872	0.0289	10.7145	0.7832	0.0286	10.4346	0.7892	0.0290
0	11.7299	0.7113	0.0248	12.45	0.7073	0.0245	11.6545	0.7133	0.0249
3	13.5375	0.5818	0.0198	13.9523	0.5778	0.0194	13.5156	0.5838	0.0198
5	14.7288	0.4941	0.0170	15.2524	0.4901	0.0165	14.7244	0.4961	0.0171
8	16.4601	0.3739	0.0137	17.1211	0.3699	0.0131	16.4228	0.3759	0.0138
10	17.5372	0.3055	0.0119	18.3306	0.3015	0.0113	17.4549	0.3075	0.0121
12	18.5405	0.2476	0.0105	19.4779	0.2436	0.0098	18.3890	0.2496	0.0107
15	19.8325	0.1791	0.0088	21.0526	0.1751	0.0080	19.5921	0.1811	0.0092

Table 3

Performance of the Proposed Model on Independent Test Sets

Noise Level (in dB)	PRED_SNR	PRD	RMSE
-12	6.3525	0.9732	0.0659
-10	7.6549	0.9560	0.0570
-8	8.9132	0.9318	0.0489
-5	10.8448	0.8738	0.0390
-2	12.9760	0.7845	0.0307
0	14.0574	0.7080	0.0271
3	15.8440	0.5789	0.0219
5	16.9562	0.4905	0.0193
8	18.7996	0.3704	0.0157
10	19.8574	0.3019	0.0140
12	20.9797	0.2437	0.0123
15	22.4349	0.1754	0.0105

where $y[t]$ and $\hat{y}[t]$ denote the clean and denoised LS signals, respectively, and N is the signal length.

4.3.3. Percent Root-Mean-Squared Difference (PRD)

The Percent Root-Mean-Squared Difference (PRD) metric assesses the recovery efficiency by comparing the input signal to the reconstructed signal. A lower PRD value indicates better reconstruction. PRD is calculated as follows:

$$\mathcal{E}_{\text{PRD}} = \sqrt{\frac{\sum_{t=1}^N (y[t] - \hat{y}[t])^2}{(y[t])^2}} \quad (9)$$

where $y[t]$ and $\hat{y}[t]$ represent the clean and denoised LS signals, respectively, and N is the signal length.

5. Results & Discussion

5.1. Ablation Study

The central question is whether models with varying attention configurations, specifically the proposed Uformer model, are optimal for this task. To assess the impact of the attention mechanisms, we use the following three model configurations for comparison:

- Uformer+: This model incorporates two attention blocks.
- Uformer: This version uses a single attention block.
- Noformer: As the name suggests, this model operates without any attention blocks.

The performance of these models was assessed across various noise levels, with metrics such as Predicted SNR (PRED_SNR), PRD, and RMSE used for evaluation using noisy LS data from ICBHI-1, ICBHI_inf-1 for training and testing purposes, respectively.

The experimental results revealed notable distinctions among the three model configurations at various noise levels. Significantly, the Uformer model, featuring a single attention block, consistently outperformed the other configurations in terms of signal-to-noise ratio (SNR) improvement, as shown in Fig. 1(f). This superiority was evident across all SNR levels, highlighting the Uformer's impressive SNR improvement performance. This trend of Uformer's dominance persisted across all noise levels, demonstrating its robustness and effectiveness across all performance criteria, i.e., PRD and RMSE.

Overall, the Uformer model exhibited substantial gains, with 4.142% higher SNR improvement, 0.647% lower PRD, and 1.698% lower RMSE on average when compared to Uformer+. Similarly, when compared with Noformer architecture, Uformer outperformed it with 4.882% higher SNR improvement, 0.967% lower PRD, and 2.305% lower RMSE

Table 4
Performance of the Proposed Model at Different SNR With Various Types of Noise

Noise Level (in dB)	Noise Type								
	Pink Noise			Heart Sound			Heart + Hospital Noise		
	PRED_SNR	PRD	RMSE	PRED_SNR	PRD	RMSE	PRED_SNR	PRD	RMSE
-12	4.582	0.971	0.058	11.625	0.953	0.027	4.624	0.969	0.062
-10	5.697	0.954	0.051	13.726	0.938	0.021	5.395	0.952	0.056
-8	6.855	0.930	0.045	13.893	0.915	0.020	5.971	0.928	0.052
-5	8.671	0.872	0.036	16.255	0.863	0.016	6.773	0.870	0.048
-2	10.520	0.783	0.029	16.687	0.779	0.015	7.561	0.783	0.043
0	11.742	0.707	0.025	18.286	0.705	0.013	8.130	0.707	0.040
3	13.480	0.578	0.020	18.470	0.577	0.012	9.141	0.579	0.035
5	14.568	0.490	0.017	19.900	0.490	0.011	9.920	0.490	0.032
8	16.091	0.370	0.014	19.832	0.370	0.010	11.286	0.370	0.027
10	17.039	0.302	0.012	21.202	0.302	0.009	12.276	0.302	0.024
12	17.936	0.244	0.011	20.727	0.244	0.009	13.322	0.244	0.020
15	19.135	0.175	0.009	22.270	0.175	0.008	14.870	0.175	0.017

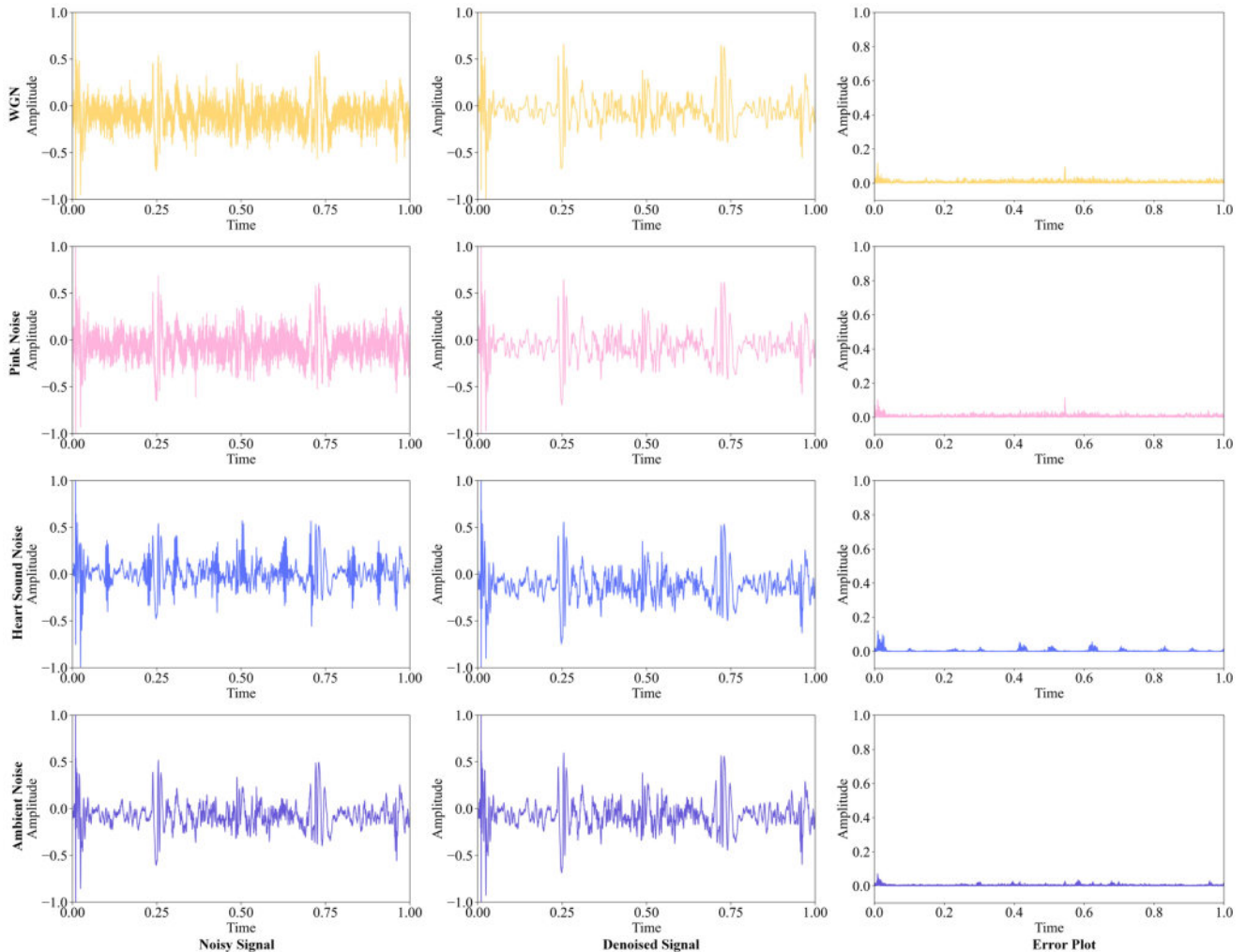


Figure 4: First column contains plots of LS signal (Fig. 2(a)) that have been corrupted with 'White Gaussian Noise (WGN)', 'Heart Sound Noise', 'Pink Noise', and 'Ambient Noise' respectively. The second column represents the corresponding denoised signals of the first column's signals using the proposed 'Uformer' architecture. The third column represents the error plots, which demonstrate the difference between the noisy signals and the denoised signals.

on average (see Table 2). These results indicated that the Uformer model, equipped with a single attention block, delivered the best denoising performance among the three configurations. This also suggests that while attention mechanisms can be advantageous for denoising tasks, the optimal number of attention blocks is crucial in achieving superior performance. The double attention block (Uformer+) and the model without any attention (Noformer) were found to be less effective in comparison to the model with a single attention block (Uformer).

Based on the experimental findings, the Uformer model with a single attention block emerges as the most optimal choice for denoising noise-corrupted lung sounds. It also underscores the efficacy of self-attention mechanisms in deep learning and the importance of configuring attention blocks appropriately to achieve optimal results.

5.2. Performance on Cross-Dataset

This section dives into the model's adaptability, examining how it fares when subjected to datasets distinct from those it was trained.

The Uformer model was initially trained on the ICBHI-1. For testing, we employed the AUH-1 dataset, introducing WGN noise to create test samples distinct from the primary datasets. To measure the model's efficacy, we relied on the same evaluation metrics as the previous section, including PRED_SNR, PRD, and RMSE.

Table 3 presents the Uformer model's performance in handling the AUH-1 Dataset, assessing its denoising capabilities across various noise levels (dB).

It underscores the model's ability to replicate its performance on datasets it has not been exposed to before. Remarkably, the model consistently surpassed the performance metrics observed on the familiar ICBHI_inf-1 test dataset (see Table 2). On the AUH-1 dataset, the model attained an average SNR improvement of 13.306 dB, in contrast to the 12.842 dB on ICBHI_inf-1. Comparable performances between AUH-1 and ICBHI_inf-1 datasets were also observed with average PRD and RMSE values of 0.6157 (PRD), 0.0302 (RMSE) and 0.6138 (PRD), 0.0267 (RMSE) respectively. A hypothesis test yielded a p-value of 0.8749, leading us to retain the null hypothesis, suggesting that the model's performance remains consistent across the independent, unseen dataset. Such findings accentuate the Uformer model's robustness and versatility, mainly when integrating a single attention block.

The evidence supports the Uformer model's ability to consistently perform well across varied datasets, each with its unique acoustic properties and recording environments. This not only testifies to the model's resilience and adaptability but also solidifies its efficacy for denoising lung sounds across an array of datasets in real-world applications.

5.3. Performance on Diverse Noise Levels and Noise Sources

In order to evaluate the effectiveness of the proposed denoising model under various noise conditions, in this

section, two primary research questions are answered: 1) Does the model generalize across different noise types? and 2) How robust is the model when confronted with noises originating from different sources? The subsequent subsections are dedicated to providing answers to these questions.

In order to answer the questions, we evaluated the proposed model across different SNRs. Originally, the Uformer model was trained using the ICBHI-1, ICBHI-2, ICBHI-3, and ICBHI-4, which were corrupted with -10dB, -5dB, 0dB, 5dB, 10dB, and 15dB. However, the evaluation expands beyond these levels to include unseen noise levels. Moreover, the Uformer model was trained and evaluated using different types of noise, such as synthetic noise (pink noise) and real-world noise, such as: heart sound noise and ambient noise (ICBHI_inf-2, ICBHI_inf-3, and ICBHI_inf-4).

Fig 1(g) presents the denoising performance of the proposed Uformer model across various SNR levels, demonstrating consistent performance even when tested on unseen SNR levels. At an input SNR of 15 dB, the improvement was 4.13 dB. As the input SNR decreased, there was a corresponding increase in SNR improvement due to the presence of high noise. Specifically, for an input SNR of 0 dB, the improvement reached 11.74 dB. Furthermore, with an input SNR of -12 dB, the model achieved an SNR improvement of 16.67 dB. These improvements are also reflected in metrics like PRD and RMSE. For an input SNR of -12 dB, the PRD and RMSE were 0.9750 and 0.0583, respectively. These values are 0.79592 and 0.04919 higher than the metrics for a 15 dB input and 0.26377 and 0.03365 higher than for a 0 dB input.

In the results presented, Table 4 enumerates the Uformer model's performance over a range of noise levels and types. The model achieved an average SNR improvement of 10.86 dB when assessed with pink noise. In tests involving heart sound and ambient noise, two common real-world noise sources, the Uformer model yielded SNR improvements of 16.41 dB and 18.27 dB, respectively. This improvement signifies the performance of the model for different types of noises. Fig. 4 visually represents various noisy signals, their corresponding denoised outputs generated by the Uformer model, and error plots illustrating the residual differences between the clean and denoised signals. From the figure, it is evident that the Uformer model effectively reduces noise across various types, with the denoised signals closely mirroring the clean signals. The minimal residuals in the error plots further underscore the model's proficiency in handling diverse noise conditions. A synthesis of the visual and numerical data clearly attests to the Uformer model's capability to denoise diverse signal types effectively.

The results presented in this section indicate that the proposed Uformer model is robust across various SNR levels and different types of noise, making it promising for real-world application. Its performance in mitigating both heart sound and ambient noise further emphasizes its utility in different noisy environments.

Table 5
Performance comparison with other SOTA methods

Noise type	Ambient Noise			Synthetic Noise(WGN)		
Noise Level	NLMS + Conv-TasNet(7)	NLMS +DINC-Net(7)	Uformer (Proposed Network)	IND-M (6)	COM-M (6)	Uformer (Proposed Network)
-6	-2.229	7.384	16.972	-	-	-
-3	-1.223	8.536	17.700	-	-	-
0	0.09	9.618	19.321	9.18	8.68	12.450
3	1.733	10.581	20.570	-	-	-
5	-	-	-	12.74	12.37	15.252
6	3.502	11.421	21.979	-	-	16.754
10	-	-	-	16.24	15.51	19.478
15	-	-	-	20.2	17.45	21.053

5.4. Comparison with State-of-the-art Models

In evaluating the Uformer model's performance and suitability for practical applications, a pivotal aspect is how it fares compared to other state-of-the-art (SOTA) architectures. This section aims to assess the Uformer model's performance compared to existing methodologies.

We extended our evaluation to include noise levels not initially used in our testing datasets to ensure a fair comparison. Specifically, we incorporated -6 dB, -3 dB, and 6 dB noisy signals, as used by Yang et al. in their work (7).

Table 5 provides a clear representation of the Uformer model's performance across various SNR levels compared to existing approaches. The existing methods primarily address two types of noise: ambient noise, as studied by Yang et al. (7), and synthetic noise (WGN), as examined by Pouyani et al. (6). The Uformer model outperforms both existing methods across all tested noise levels.

In the study by Pouyani et al. (6), they propose two models: individual (IND-M) and combined (COM-M). The IND-M model achieves a 7.09 dB SNR improvement, surpassing the 6.00 dB improvement in COM-M. However, the Uformer model, with a 9.558 dB SNR improvement, outperforms both by 34.80% and 59.23%, respectively. Notably, it is essential to point out that IND-M's training and evaluation procedure, where the network is trained with one SNR and evaluated with another, may not be realistic in practical scenarios.

In the study by Yang et al. (7), they experiment with two deep learning models: NLMS + Conv-TasNet and NLMS + DINC-Net, evaluating their performance at various SNR levels (-6 dB, -3 dB, 0 dB, 3 dB, and 6 dB). The NLMS + Conv-TasNet model performs poorly, with an average SNR improvement of 0.3746 dB. In contrast, our proposed Uformer model significantly outperforms their best-performing model, NLMS-DINC-Net, achieving an average SNR improvement of 19.3084 dB, which is nearly twice the 9.508 dB improvement exhibited by NLMS-DINC. It is worth noting that Yang et al.'s study mainly considers office, hallway, street, and similar noises as ambient noise types,

while in reality, lung sounds are corrupted by both physiological noises like heart sounds and ambient noise from the hospital environment. Our study takes this more realistic scenario into account. Additionally, when comparing the model sizes, our Uformer model has 2.00M (3.27M - 1.27M) fewer parameters than the NLMS-DINC-Net. This indicates that our model not only offers an end-to-end solution but is also a more suitable choice for integration into edge devices due to its efficiency.

The results indicate that the proposed Uformer model outperforms existing SOTA architectures in denoising lung sounds. Its significant improvements across a range of SNR levels demonstrate its superior performance, making it a promising choice for practical applications in the field.

6. Conclusions

Our paper addresses the challenge of noise cancellation during lung auscultation using electronic stethoscopes. Typically, LS signals are compromised by both convolutional and additive extraneous noises, posing a substantial obstacle to the accurate assessment of pulmonary function and the timely detection of potential diseases. Given the criticality of this issue, effective denoising emerges as an indispensable step in LS signal processing. Traditional methods of LS signal processing-based denoising typically introduce artifacts. To address this shortcoming, we introduced the Uformer, a self-attention-enabled end-to-end denoising network that delivers high SNR denoised LS signals for precise lung health assessment. The Uformer employs a two-stage encoder setup comprising a CNN and transformer encoder. This design effectively captures long-range dependencies and efficient latent feature extraction, and the CNN decoder-based architecture produces denoised signals. Our ablation study demonstrates that the Uformer surpasses models Uformer+ and Noformer, offering an average SNR improvement of 4.142% and 4.882%, respectively. In our evaluation, we assessed the model's performance against both synthetic and real-world noise scenarios to validate its resilience and adaptability. We utilized metrics such as SNR, PRD, and

RMSE for performance evaluation. Both qualitative and quantitative analyses confirm that our proposed model excels in removing various noise types, even from entirely new test datasets and noise levels. When benchmarked against SOTA denoising methodologies, the results elicited from the Uformer unequivocally highlight its marked superiority. As a future trajectory, we plan to improve the model's denoising capability to handle additional categories of sounds, including heart sounds, bowel sounds, and other physiological auscultation signals.

References

- [1] Institute for Health Metrics and Evaluation, Chronic respiratory disease is third leading cause of death globally with air pollution killing 1.3 million people, Institute for Health Metrics and Evaluation Newsroom, accessed: 2023-12-14 (4 2023).
URL <https://www.healthdata.org/news-events/newsroom/news-releases/chronic-respiratory-disease-third-leading-cause-death-globally>
- [2] S. Reichert, R. Gass, C. Brandt, E. Andrès, Analysis of respiratory sounds: state of the art, *Clinical medicine. Circulatory, respiratory and pulmonary medicine* 2 (2008) CCRPM-S530.
- [3] M. Lozano, J. A. Fiz, R. Jané, Performance evaluation of the hilbert–huang transform for respiratory sound analysis and its application to continuous adventitious sound characterization, *Signal Processing* 120 (2016) 99–116.
- [4] A. Bohadana, G. Izbicki, S. S. Kraman, Fundamentals of lung auscultation, *New England Journal of Medicine* 370 (8) (2014) 744–751.
- [5] A. Gurung, C. G. Scrafford, J. M. Tielsch, O. S. Levine, W. Checkley, Computerized lung sound analysis as diagnostic aid for the detection of abnormal lung sounds: a systematic review and meta-analysis, *Respiratory medicine* 105 (9) (2011) 1396–1403.
- [6] M. F. Pouyani, M. Vali, M. A. Ghasemi, Lung sound signal denoising using discrete wavelet transform and artificial neural network, *Biomedical Signal Processing and Control* 72 (2022) 103329.
- [7] C. Yang, N. Dai, Z. Wang, S. Cai, J. Wang, N. Hu, Cardiopulmonary auscultation enhancement with a two-stage noise cancellation approach, *Biomedical Signal Processing and Control* 79 (2023) 104175.
- [8] S. A. Baharanchi, M. Vali, M. Modaresi, Noise reduction of lung sounds based on singular spectrum analysis combined with discrete cosine transform, *Applied Acoustics* 199 (2022) 109005.
- [9] D. Singh, B. K. Singh, A. K. Behera, Comparative analysis of lung sound denoising technique, in: 2020 First International Conference on Power, Control and Computing Technologies (ICPC2T), IEEE, 2020, pp. 406–410.
- [10] F. Meng, Y. Wang, Y. Shi, H. Zhao, A kind of integrated serial algorithms for noise reduction and characteristics expanding in respiratory sound, *International journal of biological sciences* 15 (9) (2019) 1921.
- [11] M. Syahputra, S. Situmeang, R. Rahmat, R. Budiarto, Noise reduction in breath sound files using wavelet transform based filter, in: IOP Conference Series: Materials Science and Engineering, Vol. 190, IOP Publishing, 2017, p. 012040.
- [12] Y. Ding, I. W. Selesnick, Artifact-free wavelet denoising: Non-convex sparse regularization, convex optimization, *IEEE signal processing letters* 22 (9) (2015) 1364–1368.
- [13] S. Ghael, A. M. Sayeed, R. G. Baraniuk, Improved wavelet denoising via empirical wiener filtering, in: SPIE Technical Conference on Wavelet Applications in Signal Processing, 1997.
- [14] J.-P. Gallaire, A. M. Sayeed, Wavelet-based empirical wiener filtering, in: Proceedings of the IEEE-SP International Symposium on Time-Frequency and Time-Scale Analysis (Cat. No. 98TH8380), IEEE, 1998, pp. 641–644.
- [15] H. Choi, R. Baraniuk, Analysis of wavelet-domain wiener filters, in: Proceedings of the IEEE-SP International Symposium on Time-Frequency and Time-Scale Analysis (Cat. No. 98TH8380), IEEE, 1998, pp. 613–616.
- [16] N. Nikolaev, Z. Nikolov, A. Gotchev, K. Egiazarian, Wavelet domain wiener filtering for ecg denoising using improved signal estimate, in: 2000 IEEE International Conference on Acoustics, Speech, and Signal Processing. Proceedings (Cat. No. 00CH37100), Vol. 6, IEEE, 2000, pp. 3578–3581.
- [17] A. Mondal, P. Bhattacharya, G. Saha, Reduction of heart sound interference from lung sound signals using empirical mode decomposition technique, *Journal of medical engineering & technology* 35 (6-7) (2011) 344–353.
- [18] M. Molaie, S. Jafari, M. H. Moradi, J. C. Sprott, S. M. R. H. Golpayegani, A chaotic viewpoint on noise reduction from respiratory sounds, *Biomedical Signal Processing and Control* 10 (2014) 245–249.
- [19] N. S. Haider, Respiratory sound denoising using empirical mode decomposition, hurst analysis and spectral subtraction, *Biomedical Signal Processing and Control* 64 (2021) 102313.
- [20] N. S. Haider, R. Periyasamy, D. Joshi, B. Singh, Savitzky-golay filter for denoising lung sound, *Brazilian Archives of Biology and Technology* 61 (2018).
- [21] D. Emmanouilidou, E. D. McCollum, D. E. Park, M. Elhilali, Adaptive noise suppression of pediatric lung auscultations with real applications to noisy clinical settings in developing countries, *IEEE Transactions on Biomedical Engineering* 62 (9) (2015) 2279–2288.
- [22] N. Q. Al-Naggar, M. H. Al-Udini, Performance of adaptive noise cancellation with normalized last-mean-square based on the signal-to-noise ratio of lung and heart sound separation, *Journal of healthcare engineering* 2018 (2018).
- [23] J. Yin, A. Liu, C. Li, R. Qian, X. Chen, A gan guided parallel cnn and transformer network for eeg denoising, *IEEE Journal of Biomedical and Health Informatics* (2023).
- [24] Y. An, H. K. Lam, S. H. Ling, Auto-denoising for eeg signals using generative adversarial network, *Sensors* 22 (5) (2022) 1750.
- [25] P. Singh, A. Sharma, Attention-based convolutional denoising autoencoder for two-lead ecg denoising and arrhythmia classification, *IEEE Transactions on Instrumentation and Measurement* 71 (2022) 1–10.
- [26] X. Wang, B. Chen, M. Zeng, Y. Wang, H. Liu, R. Liu, L. Tian, X. Lu, An ecg signal denoising method using conditional generative adversarial net, *IEEE Journal of Biomedical and Health Informatics* 26 (7) (2022) 2929–2940.
- [27] S. N. Ali, S. B. Shuvo, M. I. S. Al-Manzo, A. Hasan, T. Hasan, An end-to-end deep learning framework for real-time denoising of heart sounds for cardiac disease detection in unseen noise, *IEEE Access* (2023).
- [28] A. Chandel, V. Kumar, P. R. Muduli, Stacked bi-1stm network and dual signal transformation for heart sound denoising, in: International Conference on VLSI, Communication and Signal processing, Springer, 2022, pp. 123–133.
- [29] Icbhi 2017 challenge, accessed: 2023-02-11 (2017).
URL https://bhichallenge.med.auth.gr/ICBHI_2017_Challenge
- [30] M. Fraiwan, L. Fraiwan, B. Khassawneh, A. Ibnian, A dataset of lung sounds recorded from the chest wall using an electronic stethoscope, *Data in Brief* 35 (2021) 106913.
- [31] B. Rocha, D. Filos, L. Mendes, I. Vogiatzis, E. Perantoni, E. Kaimakamis, P. Natsiavas, A. Oliveira, C. Jácome, A. Marques, et al., A respiratory sound database for the development of automated classification, in: Precision Medicine Powered by pHealth and Connected Health: ICBHI 2017, Thessaloniki, Greece, 18-21 November 2017, Springer, 2018, pp. 33–37.
- [32] Yaseen, G.-Y. Son, S. Kwon, Classification of heart sound signal using multiple features, *Applied Sciences* 8 (12) (2018) 2344.
- [33] S. B. Shuvo, S. S. Alam, S. U. Ayman, A. Chakma, P. D. Barua, U. R. Acharya, Nrc-net: Automated noise robust cardio net for detecting valvular cardiac diseases using optimum transformation method with heart sound signals, *Biomedical Signal Processing and Control* 86 (2023) 105272.
- [34] M. Firoozi Pouyani, M. Vali, M. A. Ghasemi, A combined model for noise reduction of lung sound signals based on empirical mode

decomposition and artificial neural network, arXiv e-prints (2022) arXiv:2209.

- [35] S. S. Alam, A. Chakma, M. H. Rahman, R. Bin Mofidul, M. M. Alam, I. B. K. Y. Utama, Y. M. Jang, Rf-enabled deep-learning-assisted drone detection and identification: An end-to-end approach, *Sensors* 23 (9) (2023) 4202.
- [36] A. Chakma, S. S. Alam, R. B. Mofidul, Y. M. Jang, Lightweight deep-learning model for rf-enabled drone detection and identification, (2023) 377–379.
- [37] M. El Helou, S. Süssstrunk, Blind universal bayesian image denoising with gaussian noise level learning, *IEEE Transactions on Image Processing* 29 (2020) 4885–4897.
- [38] Y. Zhou, J. Jiao, H. Huang, Y. Wang, J. Wang, H. Shi, T. Huang, When awgn-based denoiser meets real noises, in: *Proceedings of the AAAI Conference on Artificial Intelligence*, Vol. 34, 2020, pp. 13074–13081.
- [39] H. Ren, H. Jin, C. Chen, H. Ghayvat, W. Chen, A novel cardiac auscultation monitoring system based on wireless sensing for healthcare, *IEEE journal of translational engineering in health and medicine* 6 (2018) 1–12.
- [40] R. Nersisson, M. M. Noel, Heart sound and lung sound separation algorithms: a review, *Journal of medical engineering & technology* 41 (1) (2017) 13–21.
- [41] C. Liu, D. Springer, Q. Li, B. Moody, R. A. Juan, F. J. Chorro, F. Castells, J. M. Roig, I. Silva, A. E. Johnson, et al., An open access database for the evaluation of heart sound algorithms, *Physiological measurement* 37 (12) (2016) 2181.
- [42] D. P. Kingma, J. Ba, Adam: A method for stochastic optimization, arXiv preprint arXiv:1412.6980 (2014).
- [43] A. C. Wilson, R. Roelofs, M. Stern, N. Srebro, B. Recht, The marginal value of adaptive gradient methods in machine learning, *Advances in neural information processing systems* 30 (2017).

